Am J Physiol Heart Circ Physiol 306: H505–H516, 2014.
First published December 13, 2013; doi:10.1152/ajpheart.00655.2013.

Variation of mechanical properties and quantitative proteomics of VSMC along the arterial tree

Carla Luana Dinardo,[1] Gabriela Venturini,[1] Enhua H. Zhou,[2] Ii Sei Watanabe,[3] Luciene Cristina Gastalho Campos,[1] Rafael Dariolli,[1] Joaquim Maurício da Motta-Leal-Filho,[4] Valdemir Melechco Carvalho,[5] Karina Helena Morais Cardozo,[5] José Eduardo Krieger,[1] Adriano Mesquita Alencar,[6]* and Alexandre Costa Pereira[1]*

[1]*Heart Institute (InCor), University of São Paulo Medical School, São Paulo, Brazil;* [2]*Department of Environmental Health, Harvard School of Public Health, Boston, Massachusetts;* [3]*Institute of Biomedical Sciences, Department of Anatomy, University of São Paulo, São Paulo, Brazil;* [4]*Interventional Radiology, Vascular and Endovascular Surgery, University of São Paulo Medical School, São Paulo, Brazil;* [5]*Fleury Group, São Paulo, Brazil; and* [6]*Instituto de Física, University of São Paulo, São Paulo, Brazil*

Submitted 26 August 2013; accepted in final form 9 December 2013

Dinardo CL, Venturini G, Zhou EH, Watanabe IS, Campos LC, Dariolli R, da Motta-Leal-Filho JM, Carvalho VM, Cardozo KH, Krieger JE, Alencar AM, Pereira AC. Variation of mechanical properties and quantitative proteomics of VSMC along the arterial tree. *Am J Physiol Heart Circ Physiol* 306: H505–H516, 2014. First published December 13, 2013; doi:10.1152/ajpheart.00655.2013.— Vascular smooth muscle cells (VSMCs) are thought to assume a quiescent and homogeneous mechanical behavior after arterial tree development phase. However, VSMCs are known to be molecularly heterogeneous in other aspects and their mechanics may play a role in pathological situations. Our aim was to evaluate VSMCs from different arterial beds in terms of mechanics and proteomics, as well as investigate factors that may influence this phenotype. VSMCs obtained from seven arteries were studied using optical magnetic twisting cytometry (both in static state and after stretching) and shotgun proteomics. VSMC mechanical data were correlated with anatomical parameters and ultrastructural images of their vessels of origin. Femoral, renal, abdominal aorta, carotid, mammary, and thoracic aorta exhibited descending order of stiffness (G, $P < 0.001$). VSMC mechanical data correlated with the vessel percentage of elastin and amount of surrounding extracellular matrix (ECM), which decreased with the distance from the heart. After 48 h of stretching simulating regional blood flow of elastic arteries, VSMCs exhibited a reduction in basal rigidity. VSMCs from the thoracic aorta expressed a significantly higher amount of proteins related to cytoskeleton structure and organization vs. VSMCs from the femoral artery. VSMCs are heterogeneous in terms of mechanical properties and expression/organization of cytoskeleton proteins along the arterial tree. The mechanical phenotype correlates with the composition of ECM and can be modulated by cyclic stretching imposed on VSMCs by blood flow circumferential stress.

vascular smooth muscle; extracellular matrix; aorta; smooth muscle cells

THE FACT THAT VESSELS DIFFER SO significantly in terms of anatomic characteristics is commonly attributed to the heterogeneity of blood flow within their territories during the arterial tree development phase, which determines vessel diameter and thickness (13). In this scenario, vascular smooth muscle cells (VSMCs) orchestrate extracellular matrix (ECM) synthesis/organization and are thought to assume a quiescent contractile status after. However, VSMCs are known to play an important role in the structural modifications that some vessels undergo during pathologic conditions like atherosclerosis and hypertension (11), highlighting the fact that these cells are constantly influenced by diverse stimuli and modulate their synthetic and proliferative properties based on these stimuli. This puts into question the homogeneous quiescent mechanical status of VSMCs mentioned before.

Earlier studies have suggested that elimination of VSMC function did not significantly change the static mechanical properties of large vessels (42). Recent reports show that vessel structural modifications, such as wall rigidity, may account for the substantial contribution of the VSMC mechanical phenotype (32, 36) and that VSMC cytoskeleton proteins are positively influenced by the composition of surrounding ECM and by the pattern of local shear stress (20, 37).

VSMC location in the vascular tree changes the patterns of gene expression, mainly SMC marker genes, as well as their molecular functioning (14, 45). Considering the key role played by VSMCs in controlling ECM production and organization to maintain vessel integrity, in reorganizing vessel tunica media in the face of blood flow changes, and in regulating tissue perfusion within smaller arteries, it may be expected that their mechanical properties might vary according to the vessel of origin. Hypothetical factors that could influence VSMC mechanics and cytoskeleton organization are their embryological origin, the local blood flow, and the amount of surrounding ECM.

Based on these findings, the main objective of this study was to characterize VSMC obtained from different arterial beds in terms of mechanics and protein expression and explore if eventual differences in their mechanical profile correlate with anatomical or blood flow diversities of their vessels of origin.

MATERIALS AND METHODS

Study Design

See Fig. 1.

Vessels

Fragments of abdominal aorta, femoral, renal, mammary, carotid, coronary, and thoracic aorta arteries were collected from five same-

* M. Alencar and A. Costa Pereira contributed equally to this work.
Address for reprint requests and other correspondence: A. Costa Pereira, Avenida Doutor Enéas de Carvalho Aguiar, 44, 10th floor. Heart Institute (InCor), Univ. of São Paulo Medical School, São Paulo, SP, Brazil (e-mail: lbmpereira@incor.usp.br).

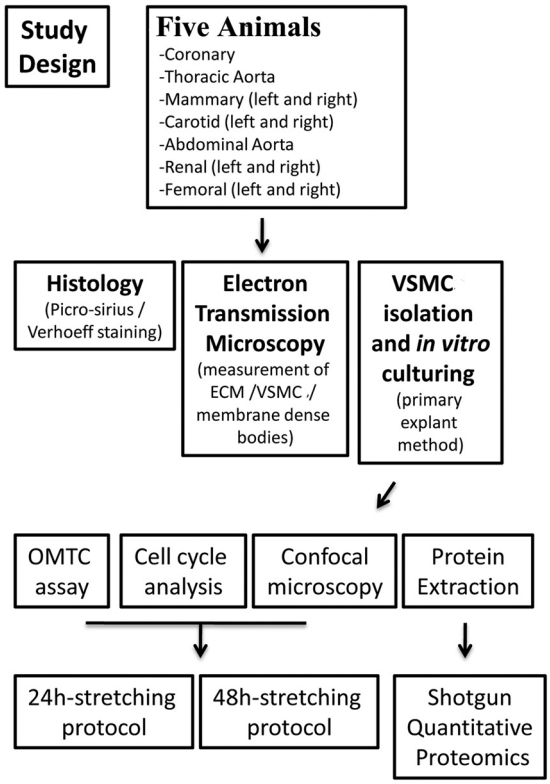

Fig. 1. The study was designed to address the mechanical phenotype of vascular smooth muscle cells (VSMCs) and its possible modulators along arterial tree. Selected arteries were anatomically evaluated using conventional Verhoeff and picrosirius staining, as well as using transmission electron microscopy (TEM). VSMC rigidity was directly accessed using optical magnetic twisting cytometry (OMTC) assay, and protein expression was evaluated using shotgun proteomics. ECM, extracellular matrix.

aged (4 mo) and -weighted female pigs (*Susscrofadomesticus*, lineage MS60 EMBRAPA, Granja RG, Suzano-SP, 15–20 kg). The animals were preanesthetized with ketamine hydrochloride (10 mg/kg) and midazolam (0.4 mg/kg), and the anesthesia was performed with sodium thiopental (10 mg/kg). Animals underwent tracheal intubation, and the anesthesia was maintained with isoflurane with 100% oxygen in a ventilator during the procedure. Saline infusion was kept throughout the procedure, and a single dose of 10,000 IU of heparin was administered. Asepsis/antisepsis was performed over the regions of interest for vessel extraction. After all vascular segments were extracted, the animals, still under anesthesia, were killed by an overdose of potassium chloride (KCl, ~30 ml). The procedure was approved according to our local ethics committee (CAPpesq–Hospital das Clínicas da Faculdade de Medicina USP-0272/11).

Cell Isolation and Culture

Fragments of the collected vessels were used to isolate VSMCs using the primary explant technique. Vessel fragments had their lumen opened and were cut into small pieces (4 × 4 mm), which were placed on a six-well plate, previously coated with 3% cutaneous porcine gelatin (catalog no. G9136; Sigma-Aldrich). Growth media used consisted of high-glucose DMEM (catalog no. 12100–046; GIBCO) supplemented with 20% fetal bovine serum (catalog no. 16000–044; GIBCO), 100 unit/ml penicillin, and 100 μg/ml streptomycin (catalog no. 15140–122; GIBCO). VSMCs were stained for alpha-smooth muscle actin (sc-53142, 1:400; Santa Cruz Biotechnology) and characterized using confocal microscopy (>95% positivity). The staining protocol was identical to that described for anti-vinculin antibody in *Confocal Microscopy*. VSMCs were expanded to subsequent passages at a 1:2 proportion. To limit VSMCs progressive softening and dedifferentiation with serial culture passaging, we performed the mechanical assay, the stretching experiment, and the acquisition of confocal images using VSMCs up to the fifth passage (10).

Cell Cycle Analysis

VSMCs (1×10^5, 4th passage) were plated in culture dishes at concentrations determined to yield 90–100% confluence. Afterwards, cells were harvested and centrifuged for 5 min at 1,699 *g* in 4°C. Subsequently, cells were washed twice with ice-cold phosphate-buffered saline (PBS), and then the supernatant was discarded, and the pellets were fixed with 1 ml of ice-cold 70% ethanol at 4°C overnight. Next, cells were centrifuged for 5 min in 4°C at 4,248 *g* and washed twice with PBS. The supernatants were withdrawn, and the cells were resuspended in 500 μl of DNA staining solution (20 μg/ml of PI, 100 μg/ml of RNase A in PBS, and 0.1% Triton-X) for 30 min at 37°C. DNA content was analyzed using FACS Caliburflowcytometry equipment (BD). The cell population in each phase of the cell cycle was determined using CellQuestPro software.

Histological Characterization of Vessels

Paraffin-embedded sections of all artery sections were stained with Verhoeff Van-Gieson (elastic stain kit, catalog no. HT25A; Sigma-Aldrich) and picrosirius red solution (catalog no. P6744; Sigma-Aldrich). Deparaffinized and hydrated sections were stained with Verhoeff solution for 1 h, rinsed (twice), differentiated in 2% ferric chloride (1–3 min), washed in tap water, treated with 5% sodium thiosulfade for 1 min, washed for 5 min, counterstained in Van Gieson solution for 3 min, dehydrated through 95% alcohol, and cleared in xylene (3 min/twice). According to the picrosirius protocol, deparaffinized and hydrated sections were stained in picrosirius red for 1 h, washed in acidified water (twice), dehydrated in 100% ethanol (3 times), and cleared in xylene.

Slides were analyzed using Leica Qwin software, and the percentage of elastic fibers (Verhoeff-stained slices) and collagen (picrosirius-stained slices) within media tunica was calculated for each vessel. Anatomical data referring to the vessel internal diameter and media thickness were calculated using the same slides. Groups were statistically compared in terms of percentage of elastin, percentage of collagen, internal diameter, media thickness, and media thickness/internal diameter ratio using one-way ANOVA. $P < 0.05$ was considered significant. The name of the vessel was not revealed to the researcher that analyzed the slices. Instead, a numerical code was given.

Transmission Electron Microscopy

Vessel fragments were preserved in modified Karnovsky solution and processed according to the methodology described by Watanabe (43). Images were acquired using Jeol-1010 equipment.

We calculated the extracellular matrix area/VSMC area ratio and the mean size of membrane-dense bodies for each selected vessel using ImageJ software. Groups were compared in terms of both variables using one-way ANOVA. $P < 0.05$ was considered significant. Data referring to dense body size underwent logarithm conversion before statistical analysis to achieve a normal distribution. Images were acquired and analyzed by two different researchers and a second one reanalyzed them to avoid subjectiveness.

Optical Magnetic Twisting Cytometry

Preparation of ferromagnetic beads. Ferromagnetic beads (4.5-μm diameter, provided by Harvard School of Public Health, Boston, MA) were covered with a synthetic peptide containing Arg-Gly-Asp (RGD) sequence (cat no. 44-0-1913; American Peptide) and suspended into a sterile carbonate buffer at a concentration of 1mg/ml.

Optical magnetic twisting cytometry experiment. VSMCs (4th culture passage) were plated on a 96-well plate (catalog no. 9102; Corning) previously coated with 3% porcine gelatin (catalog no. G9136; Sigma-Aldrich) at a concentration of 1×10^4 cells per well. Twelve hours after plating, VSMCs were serum-deprived for 24 h and then ferromagnetic beads were added at a concentration of 10 μg per well. VSMCs were then incubated for 20 min and washed once to remove loosely bound beads before the performance of mechanical measurements.

Detailed descriptions and validations of optical magnetic twisting cytometry (OMTC) have been published elsewhere (12, 31). Briefly, OMTC is a method used to measure cell viscoelasticity based on the application of a sinusoidal magnetic torque to ferromagnetic beads, which are intrinsically attached to cytoskeleton. In our experiments, beads were magnetized horizontally (9,000 Gauss) and, after, a vertical magnetic field oscillating at 0.75 Hz was put into action (90 Gauss). The resulting bead displacement was optically registered by a charge-coupled device camera mounted on an inverted microscope (Leica DMI-4000).

The ratio between the Fourier transformation of the specific torque and bead displacement defined a complex apparent stiffness of the cell, g*(f), measured in units of Pa nm^{-1}. Based on this value, it was possible to compute the elastic modulus g', the loss modulus g'', and hysteresivity η (the ratio g''/g') for the cell. The apparent stiffness g*(f) was converted into a shear modulus G* after taking into consideration the shape and thickness of the cell and the degree of bead embedding, based on previous finite-element simulations (30). G* at 0.75 Hz was labeled G. In half of experiments, contractile agonist histamine or antagonist isoproterenol were added to wells 30 s after the beginning of magnetization, and bead displacement was registered for 5 min thereafter.

VSMCs from different arteries were compared in terms of G and η. Taking into consideration a random variation between the animals, we calculated Z-score of G and η (ZG and Zη) using resultant G and η of all analyzed wells (individually for each animal). After that, the values of ZG and Zη were compared using the nonparametric Kruskal-Wallis test and $P < 0.05$ was considered significant. A Mann-Whitney test was performed as post hoc analysis, and Spearman's rank order correlation was performed to correlate variables obtained from histological analysis with ZG. We used SPSS software (17th version) in all statistical analysis.

Stretch Protocol

VSMCs were stretched using Flexcell FX-4000 cell stretching system (Flexcell International). This system applies biaxial, homogeneous tensile strains to cells cultured on silicone rubber membranes (2) and is suitable for simulating the physiological stretch applied by blood flow to most arteries (17). Then, 2×10^5 cells (5th passage) were plated in Bioflex plates previously coated with 10% porcine skin gelatin (catalog no. G9136; Sigma-Aldrich) and underwent a 10% stretch, at 1 Hz frequency, for 24 and 48 h. Control VSMCs were plated using the same protocol (also in Bioflex plates) and were kept within the same incubator as stretched VSMCs. After the end of the stretch protocol, VSMCs were harvested and prepared for OMTC experiments, as described previously. Control VSMCs were compared with stretched VSMCs using a Mann-Whitney test, and $P < 0.05$ was considered significant.

Confocal Microscopy

VSMCs were cultured on glass slides. After 48 h, cells were fixed with 4% paraformaldehyde (catalog no. 158127; Sigma-Aldrich) for 60 min, permeabilized for 30 min with 0.1% PBS-Nonidet 40 (Sigma-Aldrich), blocked overnight with 1% albumin from bovine serum (catalog no. A9418; Sigma-Aldrich) diluted in PBS, and incubated for 3 h with phalloidin conjugated with Alexa (1:400; Alexa Fluor 488 Phalloidin; Invitrogen) or for 12 h with anti-vinculin primary antibody (1:200; catalog no. V9131; Sigma-Aldrich), in this case followed by 2 h incubation with anti-mouse secondary antibody (Alexa Fluor 555 goat anti-mouse IgG, 1:500; Invitrogen). The cell nucleus was stained using 1:300 DAPI (catalog no. D9532; Sigma-Aldrich), which was added to mounting media. Fluorescence image studies were performed using a Zeiss laser-scanning confocal microscope LSM 510 META. Confocal images were acquired by one researcher, who knew their vessel of origin, but were analyzed by a second researcher after the name of the vessel had been removed and replaced by a sequential number.

ImageJ software and its plugin OrientationJ were used to analyze phalloidin-stained images regarding stress-fiber orientation, which was calculated and expressed, using as unit, the percentage of coherence: the more the fibers had a predominant orientation within the cell, the higher the coherence was. VSMCs were studied in terms of shape using ImageJ software. The variables major axis/minor axis ratio (AR) and circularity were chosen as shape descriptors, and the latter was calculated using the formula 4π (area/perimeter^2), the maximum value (one) was representative of a perfect circle and the decrease of the value towards zero reflective of cell elongation. Finally, the size of focal adhesions was calculated using vinculin-stained images and ImageJ particle analysis function.

Groups were compared in terms of stress-fiber orientation and shape-descriptors (AR/circularity) using one-way ANOVA, and $P < 0.05$ was considered significant. Femoral and thoracic aorta were compared in terms of the size of focal adhesions (vinculin-stained images) using Student *t*-test, and $P < 0.05$ was considered significant.

Proteomics

Protein extraction. Five aortic cell plates and six femoral cell plates with 1.0×10^6 cells were extracted with 100 μl of extraction buffer and mechanical lysis. Proteins were centrifuged at 16,000 *g* for 15 min at 4°C. The supernatant was then quantified in triplicate using the Bradford protein assay (Bio-Rad no. 500–0201) according to manufacturer's specifications.

Protein digestion. The protein digestion was carried out according to Camargo et al. (5) with a few modifications. Different from Camargo et al., we diluted 50 μg of total protein in 50 mM ammonium bicarbonate to a final volume of 60 μl, whereas Camargo et al. diluted in Milli-Q water to a volume of 30 μl. We used 21 μl of the internal standard (yeast alcohol dehydrogenase-P00330 at 1 pmol/μl) whereas Camargo et al. used 5 μl of the internal standard at 250 fmol/ml. Briefly, 50 μg of total protein were diluted in 50 mM ammonium bicarbonate to a final volume of 60 μl. The protein samples were denatured with 0.2% (wt:vol) RapiGest SF for 15 min at 80°C, reduced with 2.5 μl of 100 mM dithiothreitol at 60°C for 30 min, alkylated with 2.5 μl of 300 mM iodoacetamide at room temperature, and enzymatically digested at 37°C overnight with trypsin at a 1:100 (wt/wt) enzyme:protein ratio. Then, 10 μl of 5% trifluoroacetic acid were added to the digestion mixture to hydrolyze the RapiGest, and the samples were incubated at 37°C for 90 min. The tryptic peptide solution was then centrifuged at 16,000 *g* for 30 min at 6°C, and the pH of the supernatant was adjusted to 9.8 by the addition of 5 μl 1 M NH_4OH. Finally, 21 μl of the internal standard (yeast alcohol dehydrogenase-P00330 at 1 pmol/μl) were added to the resulting solution.

Two-dimensional liquid chromatography/mass spectrometry analysis. Separation of peptides was performed using two-dimensional high performance liquid chromatography (2D-HPLC) employing reversed-phase in both dimensions. Separation was achieved using pH 9.8 in the first and pH 2.6 in the second LC dimension. The separation at pH 9.8 was performed in off-line mode on Acquity UPLC I-Class system equipped with photodiode array (PDA) detector (Waters, Manchester, UK), with Gemini NX 3 μm 50 × 2.0 mm column mobile phase were ammonium formate in water, 20 mM, pH 9.8 and acetonitrile. Eight fractions of 0.5 min each were automatically collected and were evaporated. The final pellet was resuspended in 50 μl of 0.1%

trifluoroacetic acid in 5% acetonitrile. Each fraction was injected into a second LC dimension through a nanoACQUITY system (Waters). The samples were first trapped in a Symmetry C18 5 μm, 180 mm × 20 mm column (Waters) with 0.1% TFA in 3% acetonitrile, then peptides were eluted from the trap column to a HSS T3 1.8 μm, 75 μm × 15cm analytical column (Waters) using as mobile *phase A*: water with 0.1% formic acid and *B*: 0.1% formic acid in acetonitrile.

Mass spectrometric acquisition was achieved in a Synapt MS Q-TOF mass spectrometer equipped with a NanoLockSpray source in the positive ion mode (Waters). For all measurements, the mass spectrometer was operated in the "V" mode with a typical resolving power of at least 12,500. Data-independent scanning (MSE) experiments were performed by switching between low (3 eV) and elevated collision energies (15–50 eV) applied to the trap "T-wave" cell filled with argon. Scan times of 0.8 s were used for low- and high-energy scans from m/z 50 to 2000.

Protein identification and database analysis. Protein identification was performed in Global Server v.2.5 (PLGS) with human UniProtKB Complete Proteome database. Maximum missed cleavages by trypsin allowed were up to 1, fixed modification by carbamidomethylation (cistheine), and variable modifications by acetyl NH_2-terminal and oxidation (methionine) were considered. Label-free quantification was obtained by the PLGS processing, and the lists of identified and/or quantified proteins in each condition (aortic and femoral) were performed.

Statistical analysis. The data were analyzed using the Student *t*-test and fold change to assess differences between aortic and femoral cells with statistical significance ($P < 0.05$ and fold change >1.5). Network analyses were performed using MetaCore version 6.14 (http://portal.genego.com).

RESULTS

Structural Characterization of the Vessels

Studied vessels (coronary, thoracic aorta, mammary, carotid, abdominal aorta, renal, and femoral) differed in terms of thickness ($P < 0.001$), internal diameter ($P < 0.001$), thickness/internal diameter ratio ($P < 0.001$), percentage of elastin ($P < 0.001$), and percentage of collagen ($P = 0.02$), both measured within tunica media (Fig. 2). Descriptive data are available in the Table 1.

The content of elastin decreased significantly as the vessels moved away from the heart, consistent with previous observations (35), and the thoracic aorta exhibited the highest percentage of elastin (Fig. 2, *A* and *C*). The thickness/internal diameter ratio was significantly higher in abdominal aorta branches (femoral and renal arteries) compared with the abdominal aorta itself and to thoracic vessels (thoracic aorta, mammary, and coronary; $P < 0.001$; Fig. 2*B*). Differences found regarding internal diameter and media thickness were striking because of the higher dimensions of the thoracic aorta. Even though the percentage of collagen was different among the vessels, a pattern for this variation has not been identified.

The proportion of ECM within tunica media of different vessels was calculated using transmission electron microscopy (TEM) images and was expressed as the ratio ECM area/VSMC area. The thoracic aorta exhibited the highest amount of ECM surrounding VSMCs, followed by the mammary artery (Fig. 2*D*). The thoracic aorta and mammary ECM/VSMC ratio was approximately times higher than the highest ECM/VSMC ratio of the infra-diaphragm arteries (abdominal aorta, renal, and femoral; $P < 0.001$; Fig. 2*D*). As well as the higher amount of ECM, the thoracic aorta and mammary also exhibited less aligned VSMCs compared with femoral and renal arteries (Fig. 2*E*).

Our results regarding the structure of different arteries were consistent with previous data from literature, which show that elastin predominates in the thoracic aorta and decreases significantly in the extra thoracic arteries, followed by an increase in both the elastic modulus and the pulse wave velocity (16). Also, vessel diameters were proportional to those previously described for humans (33). Considering the striking differences regarding distance from the heart and ECM composition between the thoracic aorta and femoral artery, those vessels were chosen to be contrasted in some of our analysis.

Morphometric Analysis of VSMCs and Membrane Dense Bodies

As a step before the mechanical evaluation of VSMCs, we chose to directly access their membrane dense bodies (MDB) using TEM, as the ultrastructural evaluation allowed us to most closely visualize VSMCs as they were arranged in vivo, especially regarding the linkage to ECM. MDB (focal adhesions) anchor actin filaments to plasma membrane, influence SMC cytoskeleton remodeling and linkage to ECM, and may be directly related to vessel rigidity (19, 36). MDB mean size was significantly different between VSMCs from different territories ($P < 0.001$): femoral had the largest MDBs, and thoracic aorta had the smallest (Fig. 3, *A*-*C*). To evaluate if this difference regarding focal adhesion area was persistent in vitro, we have analyzed vinculin-stained immunofluorescence images of VSMCs and the results were consistent: VSMCs from the thoracic aorta presented with significantly smaller focal adhesions compared with VSMCs from the femoral artery (Fig. 3, *F* and *G*). As larger MDB/focal adhesions are positively associated with greater cell rigidity, this finding highlights that femoral VSMCs may have a different final mechanical behavior compared with other arteries, especially regarding cytoskeleton organization and linkage to ECM.

Phalloidin-stained confocal images were studied regarding VSMC shape and actin stress-fiber orientation (Fig. 3, *D* and *E*). We decided to evaluate VSMC shape based on previous observations that have correlated the morphology of VSMCs and their phenotype: spindle-shaped VSMCs were always associated with a more differentiated phenotype (contractile) compared with rhomboid SMCs (proliferative) (15, 38). In our analysis, VSMCs were morphologically different ($P < 0.001$, for both AR and circularity): femoral and coronary VSMCs were more elongated compared with VSMCs from the other vessels (Fig. 3*D*). We did not find a significant difference regarding stress-fiber orientation between the vessels ($P = 0.242$).

Cell-Cycle Analysis

VSMCs obtained from different arteries were subjected to cell-cycle analysis. VSMCs cultured in vitro were homogeneous in terms of percentage of cells within each stage of the cell cycle, irrespective of their vessel of origin (Fig. 4). We identified, on average, 0.89 ± 0.34% cells in G_0-G_1, 73.28 ± 9.2% in S phase, 3.99 ± 1.6% in G_2, and 12.21 ± 5.7% in sub-G_0.

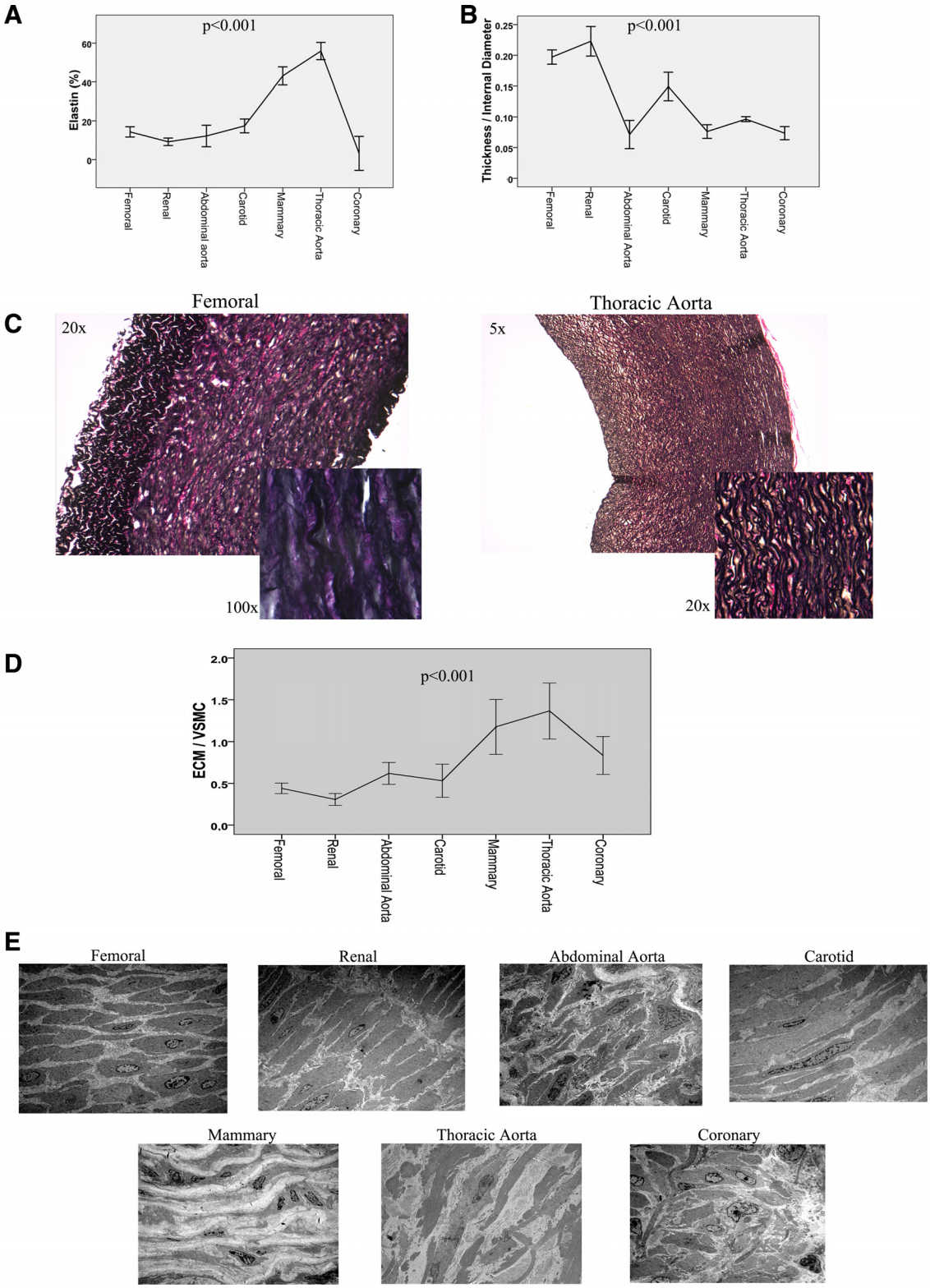

Fig. 2. Structural characterization of studied arteries. *A*: amount of elastin within tunica media decreased as vessels moved away from heart. Thoracic aorta presented with the highest amount of elastic fibers, while femoral and renal arteries presented the lowest ones. In the graph, arteries are disposed in descending order of distance from the heart. Points: mean value; error bars: 95% confidence interval. *B*: thickness/internal diameter ratio was higher in the branches of the abdominal aorta, compared with thoracic vessels. Points: mean value, error bars 95% confidence interval. *C*: Verhoeff Van-Gieson staining of femoral and thoracic aorta. Thoracic aorta presented the highest thickness and the highest amount of elastin within its media layer, compared with all other vessels. Femoral and thoracic aorta are compared in terms of tunica media thickness (main pictures) and in terms of percentage of elastin (smaller pictures, in which elastic fibers are stained in deep purple). *D*: amount of ECM surrounding VSMC was lower in heart-distant femoral and renal arteries compared with thoracic aorta and mammary arteries. Transmission Electron Microscopy (TEM) images of all vessels (*E*) clearly expose that difference and also highlights that femoral and renal VSMCs are more aligned than thoracic aorta and mammary VSMCs.

Table 1. *Anatomical and structural differences of studied vessels*

	Femoral	Renal	Abdominal Aorta	Carotid	Mammary	Thoracic Aorta	Coronary
Media thickness, μm	324 ± 21	207 ± 39	318 ± 16	270 ± 42	142 ± 21	1,242 ± 56	94 ± 10
Internal diameter, μm	1,645 ± 12	944 ± 134	4,500 ± 500	1,896 ± 340	1,924 ± 244	12,876 ± 251	1,284 ± 90
Thickness/internal diameter	0.2 ± 0.01	0.22 ± 0.04	0.071 ± 0.01	0.149 ± 0.04	0.076 ± 0.02	0.096 ± 0.002	0.074 ± 0.01
Colagen, %	12.78 ± 6.57	24.17 ± 5.63	12.76 ± 3.82	22.34 ± 8.45	14.7 ± 3.5	18.13 ± 3.9	19.23 ± 9.9
Elastin, %	14.3 ± 2.9	9.2 ± 3.5	12.2 ± 4.5	17.4 ± 5.3	43.1 ± 7.7	56 ± 2.8	3.2 ± 1
ECM/VSMC ratio	0.44 ± 0.09	0.31 ± 0.09	0.62 ± 0.2	0.53 ± 0.22	1.18 ± 0.35	1.4 ± 0.27	0.83 ± 0.3

Data are expressed as means ± SD. ECM, extracellular matrix; VSMC, vascular smooth muscle cell.

Mechanical Characterization of VSMCs

VSMCs from different arteries were evaluated using OMTC assay. We performed the following number of valid OMTC experiments: 51 (renal), 33 (abdominal aorta), 49 (femoral), 51 (mammary), 63 (carotid), 16 (coronary), and 33 (thoracic aorta). An experiment was considered valid if the following conditions were met: *1*) VSMCs were confluent, *2*) a minimum of 150 ferromagnetic beads were identified within the well, and *3*) VSMCs exhibited a regular morphology pre- and post-OMTC experiment.

VSMCs differed in terms of G among the different arterial beds, being the results consistent in all analyzed animals. The Z-score of G was calculated for each artery (ZG), as exposed in MATERIALS AND METHODS, and a significant difference was found ($P < 0.001$; Fig. 5*A*). The thoracic aorta exhibited the lowest value of ZG and femoral artery exhibited the highest ones ($P < 0.001$; Fig. 5*A*). In a more comprehensive analysis, thoracic aorta VSMCs exhibited significantly lower ZG than VSMCs from infra-diaphragm vessels (abdominal aorta, renal, and femoral arteries; $P < 0.001$), reflecting a less rigid behavior of VSMCs originating from that vessel. Regarding vessel distance from the heart, a clear tendency of ZG elevation with the increase of that distance was observed (Fig. 5*A*). This statement does not apply to the coronary artery, which receives blood irrigation during diastoles. The η median Z-score (ηZ) did not statistically differ between the different vessels, meaning that histeresivity did not change significantly between the VSMC ($P = 0.115$).

In all experiments with histamine, regardless of the animal, an increase of G after the addition of drug was observed and was reflected by a median normalized G (final postdrug G/basal predrug G) of 1.604 (interquartile range: 0.559). Response to isoproterenol was more heterogeneous (median normalized G of 0.816; interquartile range: 0.416) and significantly varied between animals ($P < 0.001$). This behavior has already been described elsewhere (47) and may reflect the amount of beta-receptors present within cell membrane. VSMCs from different vessels did not differ regarding their intensity of response to both antagonists and agonists drugs ($P = 0.327$ for histamine and $P = 0.234$ for isoproterenol).

Identification of Possible Modulating Factors of VSMCs Mechanics

After the recognition that VSMCs static rigidity varied according to their position in the arterial tree, we studied whether the ECM composition and the cyclic deformation of the arterial wall due to blood flow had any influence on this behavior.

Correlation between ECM data and VSMC rigidity. When OMTC results are contrasted with our previous presented vessels anatomic data, it is clear that VSMCs from arteries with less elastic fibers and less surrounding ECM (femoral and renal) were stiffer compared with the thoracic aorta VSMCs (elastin and ECM-rich). We found a strong negative correlation between the vessel percentage of elastin and the VSMC rigidity (ZG; $P < 0.01$, correlation coefficient: -0.724 and $r^2 = 0.524$) and between the ECM/VSMC ratio and the VSMC rigidity (ZG; $P < 0.01$, correlation coefficient: -0.847 and $r^2 = 0.718$). Femoral VSMC higher rigidity was consistent with our previous observations that those cells presented larger MDB in ultrastructural analysis.

VSMC mechanical behavior after prolonged stretching. Our main objective with this experiment was to verify if cyclic circumferential stress applied over artery walls could influence VSMC mechanical behavior and not to reproduce each vessel-specific stretching condition. We chose the 10% intensity/1-Hz rate protocol, as it is classically considered as physiological (7, 22) and has proven to reproduce an arterial regimen (6).

VSMCs from each studied vessel underwent cyclic stretching (10%, 1 Hz) for 24 and 48 h. Each experiment was repeated twice, on different occasions and with VSMCs from different animals, to guarantee reproducibility. We performed the following valid OMTC experiments after 24 h of stretching/48 h of stretching: 12/12 (carotid), 12/9 (femoral), 12/12 (renal), 12/8 (abdominal aorta), 12/8 (thoracic aorta), and 12/8 (coronary). The same number of control experiments was done.

The 24-h-stretched VSMCs from the mammary artery were less stiff compared with their static controls ($P < 0.001$; Fig. 5*B*). VSMCs from other vessels did not significantly change their elastic behavior after 24 h of stretching. By contrast, after 48 h of stretching, VSMCs from all vessels were less stiff compared with controls and the magnitude of G reduction, expressed in terms of normalized poststretching G (G of poststretched VSMCs/median G of control wells), was similar for all vessels ($P = 0.675$; Fig. 5*B*).

Comparison of Protein Expression Between VSMCs with Different Rigidity Using Shotgun Proteomics

VSMCs from the thoracic aorta and femoral artery, which had highly heterogeneous mechanical behaviors, were quantitatively compared using shotgun quantitative proteomics (Fig. 6). This methodology was chosen based on its high sensitivity and reproducibility in profiling protein content in biological samples and, in our case, in comparing two different dynamic proteomes, as well as due to its high-throughput capacity. A total of 1,628 proteins were quantified and/or identified, of which 232 were exclusively identified in aorta VSMCs, 168

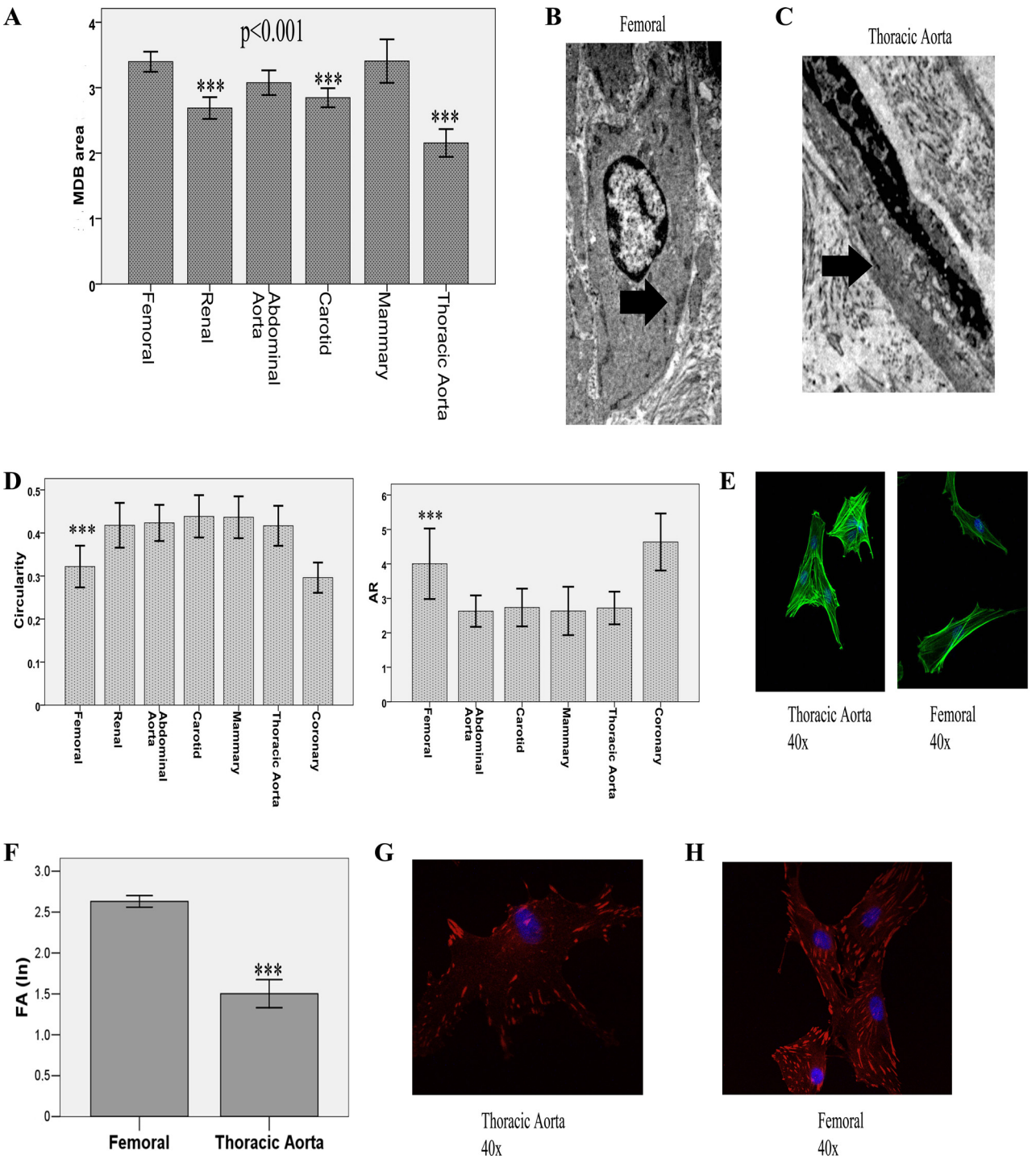

Fig. 3. VSMCs from different arteries were significantly different in terms of shape and membrane dense body dimensions (MDB; ANOVA, $P < 0.001$). *A*: femoral VSMC had an average area of MDB significantly larger than the other vessels. Graph: bars represent logarithm conversion of MDB area and error bars represent 95% confidence interval. Asterisks mark post hoc comparisons of the arteries in relation to the femoral artery. *B*: ×2,500 TEM image of femoral VSMCs. Arrow point: one MDB. *C*: ×5,000 TEM image of thoracic aorta VSMCs. Arrow point one MDB. *D*: femoral VSMCs were more elongated than the others (except for coronary). In the first graph, the studied variable was circularity and, in the second graph, major axis/minor axis ratio (AR). Bars represent mean and error bars represent 95% confidence interval. *E*: confocal images of femoral and thoracic aorta VSMC stained with phalloidin. Femoral VSMC are more elongated than thoracic aorta VSMC. Both the size of MDB and the VSMC shape may have an influence on their final mechanical behavior. These results highlight that femoral VSMC differently organize the cytoskeleton. *F*: in vitro size of focal adhesions (FAs) was compared between VSMCs from femoral and thoracic aorta arteries using vinculin-stained immunofluorescence images (*G* and *H*, red: vinculin, blue: nucleus). Consistent with our previous results using TEM images (*A*), the thoracic aorta presented significantly smaller FAs compared with the femoral artery (*F*, bars: mean value of FA area after logarithm conversion, error bars: 95% confidence interval).

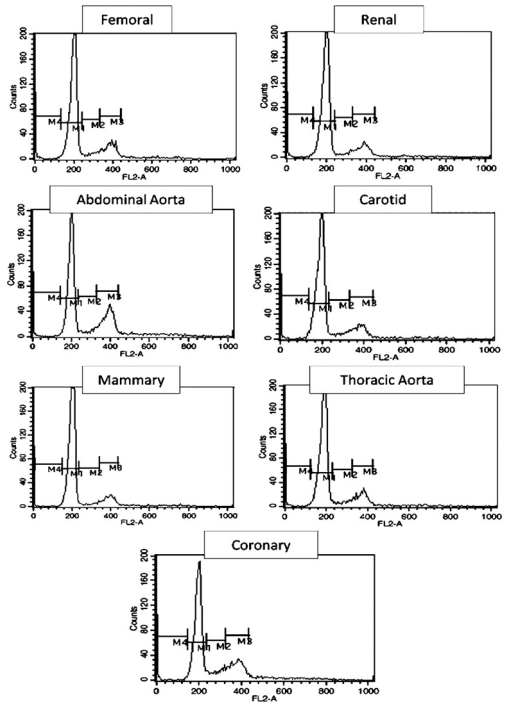

Fig. 4. Histograms representing cell cycle analysis of VSMCs from all arteries. M1: phase G_0-G_1; M2: phase S; M3: phase G_2; and M4: phase sub-G_0. Percentage of cells within each phase of the cell cycle was homogeneous, irrespective of the vessel of origin.

exclusively identified in femoral VSMCs, and 1,233 were identified in both groups (Fig. 6*A*). Quantified proteins were submitted to statistical analysis, 10 proteins were overexpressed in aorta VSMC group and 3 overexpressed in femoral VSMC group ($P < 0.05$, Fig. 6*C*).

Based on enrichment analysis, aorta expressed significantly higher amounts of proteins related to the biological processes of contraction and cytoskeletal organization (Fig. 6*C*). Proteins involved in the cytoskeletal biological network, mainly regarding regulation of cytoskeleton rearrangement and actin filaments, were strikingly more expressed in VSMC from the aorta than in those from the femoral artery. In statistical analysis, we identified the differential proteins of the aorta as microtubule-associated protein, α-actinin 4, fructose-bisphosphatealdolase A, vinculin (isoform 2), α-actinin 2, actin, 22-α smooth muscle protein, malate dehydrogenase, phosphoglycerate mutase-1, and protein DJ-1.

Of these differential proteins, actin stands out as the most important structural cytoskeletal protein, directly responsible for cell deformability and integrity, followed by microtubule-associated protein. The increased expression of actin by aorta VSMCs was accompanied by an also increased expression of proteins involved in the organization of actin stress fibers (α-actinin and vinculin isoform 2). Those "organizer" proteins form VSMC dense bodies/focal adhesions, which play an important role in determining cell mechanics through rearrangement of actin fibers. The impression is that aorta VSMC protein machinery is intensely dedicated to meeting the continuous need of cytoskeleton reorganization due to cyclic fluidization and re solidification of cell cytoplasm.

Femoral differential proteins (quantitatively most different from aorta) were related to the cell cycle network. Based on our cell-cycle analysis, this finding does not mean that femoral VSMCs have a higher replicative behavior than aorta VSMCs, but maybe this reflects that different levels of proteins are required to achieve a similar rate of replication in different environments, as previously observed (18).

DISCUSSION

Our results point out that VSMCs from different vessels of the arterial tree differ in terms of mechanical phenotype: VSMCs from the thoracic aorta are significantly less rigid than VSMCs from heart-distant renal and femoral arteries. VSMC rigidity was lower in the vessels with the higher percentage of elastin and higher amount of ECM, suggesting a common modulator for all parameters or an influence of ECM on VSMC rigidity. Cyclic stretching of VSMCs (simulating elastic artery regimens) led to homogeneous reduction of their rigidity. This finding highlights the finding that regional mechanical forces have an influence on VSMC mechanics independent of ECM cross-signaling and that some interarterial static differences regarding this phenotype may be due to the intensity of cyclic wall deformation imposed by blood flow. The amount of cytoskeletal proteins expressed in VSMCs with extreme compliant behavior (thoracic aorta) was significantly higher than that present in their stiffer opponent (femoral), which expressed more proteins involved in the cell cycle process. This may be reflective of different regional mechanical stresses and ECM composition, which influence VSMC cytoskeletal organization.

The present study is the first to confirm the heterogeneity of VSMCs mechanics along arterial tree through direct measuring of cytoplasm rigidity and through evaluation of global protein

Fig. 5. VSMC rigidity varied according to the position in arterial tree (Z-score G and G, Kruskall-Wallis, $P < 0.001$). *A*: Z-scores of the variable G for each artery are disposed in the first graph and, in the second graph, raw data (G) is presented. In both graphs, arteries are displayed in descending order of distance from the heart (femoral, renal, abdominal aorta, carotid, mammary, thoracic aorta, and coronary), and an increase in VSMC rigidity as their vessel of origin moves away from the heart is noticed. When those mechanical data are interpreted taking into consideration previously exposed vessel anatomy, it is clear that VSMCs from arteries with less elastic fibers and less surrounding ECM (femoral and renal) were stiffer compared with the thoracic aorta VSMCs. In both graphs, asterisks mark the post hoc comparisons of the arteries in relation to the femoral artery. *B*: to evaluate if mechanical differences found between VSMCs from different arteries were due to the differences in regional mechanical forces, we subjected cells to 24- and 48-h-cyclic stretching protocol. After 24 h of stretching, only mammary VSMCs acquired a less rigid behavior. However, after 48 h of stretching, all VSMCs were less rigid compared with their controls (black bars represent median G of control non-stretched VSMC and gray bars represent median G of stretched VSMC, error bars are 95% confidence interval). *C*: as it was demonstrated that cyclic stretching is a regulator of VSMC mechanical phenotype, we compared VSMC rigidity after 48-h stretching between 4 different vessels (femoral, renal, carotid, and thoracic aorta) to evaluate if the mechanical differences we initially found persisted after a course of peristalsis, which would represent a more physiological in vitro model. We chose four vessels to assure that VSMC were stretched within the same experiment, avoiding biased comparisons. The persistence of mechanical differences between VSMCs from different origins is shown in the graph, in which asterisks mark the post hoc comparisons of the arteries in relation to the femoral artery. This finding reinforces that VSMC rigidity varies according to their position in arterial tree.

expression, as well as the first to identify regional forces and ECM as possible modulating factors of this specific phenotype. Previous studies that have addressed the heterogeneity of SMCs from different origins mostly compared VSMCs with visceral SMCs (23) or arterial VSMCs vs. venous VSMCs (28) and relied mainly on evaluating expression of SMC marker genes and their transcription factors (45).

The observation that VSMCs are mechanically different along arterial tree is indeed relevant, as it goes against indiscriminate labeling of VSMC mechanical and synthetic behav-

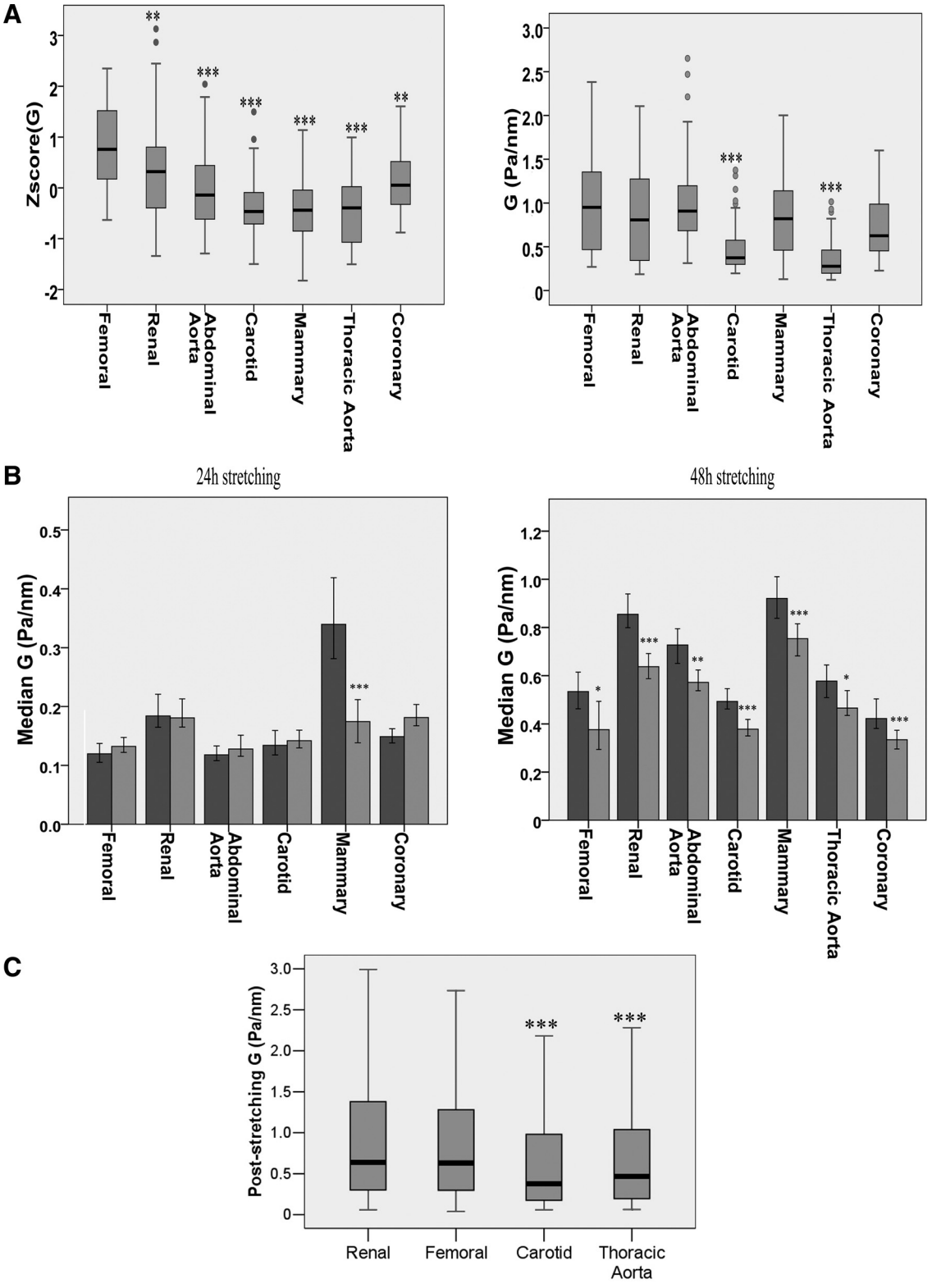

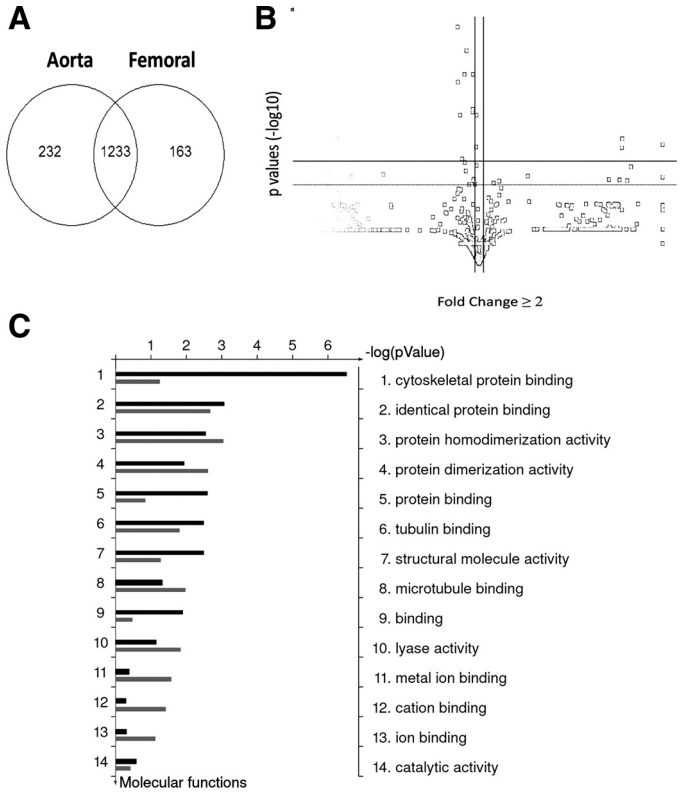

Fig. 6. Aorta VSMCs were compared with femoral VSMCs using quantitative shotgun proteomics. *A*: 1,628 proteins were identified/quantified (232 exclusively in aorta VSMC and 168 exclusively in femoral VSMC). *B*: volcano plot analysis: 10 proteins were overexpressed in aorta VSMC and they were mainly related to the cytoskeleton structure and organization ($P < 0.05$). *C*: molecular functions of aorta differential proteins are quantitatively exposed in this graph (black: aorta VSMC, gray: femoral VSMC). The amount of proteins related to cytoskeleton organization expressed by aorta VSMC was strikingly higher than that expressed by femoral VSMC. This finding is consistent with our results showing the dichotomous mechanical behavior of VSMC from these 2 territories.

iors, both in physiological and pathological situations. VSMCs from different vessels synthesize ECM quantitatively and qualitatively heterogeneously, depending on the regional blood flow during the arterial tree development phase. After this period, VSMCs classically assume a quiescent, low-proliferative and contractile phenotype (29). Considering that static VSMC mechanics are considerably variable among different arteries, classifying all of them as "contractile" does not seem to be correct. Even the concept of "phenotypic switching," commonly used to explain the assumption of a more proliferative and synthetic behavior of VSMCs in pathological situations (19), needs to be considered carefully, as it does not foresee heterogeneous cell mechanics and, consequently, does not take into consideration a plausible heterogeneity in this process along the arterial tree.

The embryological origin of vessels is always pointed out as one of the things responsible for VSMC phenotypical diversity, as cells from vessels of distinct embryological origin differ in terms of morphology, growth, and response to growth factors (40). Differences regarding VSMC mechanical behavior, as demonstrated by our results, may also be related to the embryological origin of the vessels: thoracic aorta and mammary, whose VSMCs were less rigid, are para-axial mesoderm and cranial neural crest derived, while the abdominal aorta and its branches, whose VSMCs were more elastic, are derived from splanchnic mesoderm. However, based on our results, ECM and circumferential stress also play a role in determining VSMC mechanical phenotypes.

We found a clear correlation between VSMC rigidity and the amount/composition of ECM within the media layer. There was a negative correlation between the amount of medial ECM and VSMC rigidity, the thoracic aorta being the vessel with the greatest amount of surrounding ECM and with the least elastic VSMC. The progressive decrease in elastin content as vessels moved away from the heart was accompanied by an increase in VSMC rigidity towards the same direction. One hypothesis is that VSMC mechanical phenotype may be influenced by ECM properties. Indeed, elasticity and thickness of ECM are known to influence cytoskeletal organization and cell mechanics: rigid ECM leads to formation of large and stable focal adhesions, whereas soft matrices lead to the establishment of transient ones (4, 36). Our ultrastructural analyses of VSMCs are in accordance with these previous observations, as cells from the thoracic aorta (higher amount of elastin) exhibited smaller focal adhesion compared with cells from the femoral artery (lower amount of elastin).

The presence of elastin within ECM has been previously demonstrated to regulate VSMC functioning, as it positively influences VSMC cytoskeletal organization and negatively influences their proliferative rate (20). In our analysis, we found neither significant differences regarding stress fiber orientation between the territories, nor significant differences regarding proliferative behavior. Even though cell adhesion to ECM is known to regulate cytoskeleton organization mainly through focal adhesion plasticity (36) an alternative explanation to our findings is that, as VSMC secrete ECM during development, the correlation of composition/amount of ECM and VSMC mechanics may be reflective of a common modulator of both parameters.

Circumferential stress applied towards the vessels by blood flow influences VSMC mechanical heterogeneity, as chronic cyclic axial stretching at a fixed intensity was able to change static VSMC rigidity in our experiments, this response being homogeneous for all studied vessels. Stretching conditions simulated in our experiments are best compared with the condition that VSMCs from elastic vessels undergo during physiological situations. VSMCs from the thoracic aorta, which undergoes the most intense circumferential stress, exhibited a static compliant profile. Femoral and renal VSMCs, which were more rigid, assumed a more compliant static behavior after cyclic stretching, shedding light on circumferential stress as a determinant of VSMC mechanical heterogeneity.

Cyclic stretching is known to stimulate some SMC signaling pathways (GTPase Rac, protein kinase A, protein kinase, and p38 mitogen-activated protein kinase) (21, 27) and to increase both the ECM synthesis (26) and the expression of SMC contractile marker-genes proteins (alpha-actin, sm-22, calponin, and smooth muscle myosin heavy chain) (38). Also, stretching may lead to reorientation of stress fibers, depending on the cell type, substrate characteristics and intensity of deformation (9) and may change VSMC proliferative behavior (7). However, most studies assess the final results of cyclic stretching-induced cytoskeletal reorganization. It must be highlighted that, to fluidize and resolidify their cytoplasm during

cyclic deformation, VSMCs suffer assembly/disassembly of their stress fibers, as well as growth and disruption of focal adhesions (36). Therefore, the process is much more dynamic.

Our proteomics analysis of VSMCs with opposing mechanical behaviors (thoracic aorta and femoral) clearly demonstrates that these cells quantitatively differ in terms of proteins involved in the processes of muscle contraction and cytoskeleton organization. VSMCs from the thoracic aorta expressed a significantly higher amount of cytoskeleton proteins, both constituents of cytoskeleton structure itself (actin, microtubule-associated protein) and members of focal adhesions (vinculin, alpha-actinin). On the contrary, VSMCs from the femoral artery expressed significantly more proteins involved in cell cycle network. As presented earlier, the thoracic aorta's VSMC had a static mechanical behavior more compliant than femoral VSMCs, and in ultrastructural analysis the thoracic aorta had significantly smaller membrane focal adhesions. Both thoracic aorta and femoral arteries had similar amounts of cells in each stage of cell cycle. The common sense understanding would be that VSMCs with higher amounts of cytoskeletal proteins have a more rigid cytoplasm and that VSMCs with higher amounts of cell cycle proteins proliferate more. In our observations, this extrapolation proved not to be true, and carefully studying cell physiology before the interpretation of any proteomics data is essential to avoid inaccuracies.

The organization of actin stress fibers is highly dynamic and involves a large array of actin-binding proteins and focal-adhesion associated proteins, which regulate stress fibers assembly and stability, allowing cells to properly adapt to different mechanical forces (39). Even if the amount of actin is kept constant, cytoplasm rigidity can change due to modifications in the rate of stress fiber assembly (44) and focal adhesion enlargement, which is dependent on mechanical stress (34, 36). In our results, VSMCs from the aorta were less rigid than VSMCs from femoral, but the former presented with smaller focal adhesions. Even though we could not detect differences regarding stress fibers alignment, VSMCs from aorta and femoral were heterogeneous regarding their shape, which may indirectly reflect their cytoskeleton organization.

Based on previous observations of Trepat et al. (41) and Chen et al. (8), cell response to stretch is cytoplasm fluidization. Considering mechanical forces imposed by blood flow in the thoracic aorta, VSMCs from this area experience both fluidization during systole and resolidification during diastole. The quick and effective reorganization of the cytoskeleton, especially through focal adhesion plasticity, allows VSMCs to meet ECM cyclic deformation due to circumferential stress. As this process may be less intense in peripheral arteries, it may justify the lower expression of proteins related to cytoskeletal organization within their VSMCs.

Finally, the contribution of VSMC rigidity to the resultant mechanical property of any vessel has always been considered nonsignificant (1). This concept has recently begun to change, as there is evidence that senescent arterial rigidity may be due to the stiffening of VSMCs (32), that selective removal of VSMCs from tunica media may alter vessel morphology (24), and that mutations in the myosin heavy chain (MYH11) may alter aorta contractility due to modifications in the VSMC cytoskeleton (25). In our experiments, VSMC-measured rigidity was consistent with previously described compliance and ECM elasticity of their vessels of origin, so that a more rigid behavior was observed in VSMCs from more rigid vessels that exhibited lower elastin content. However, a causal relationship cannot be established, as this subject was not addressed directly in the present study.

Our study has some limitations. The first is that the regulatory function that endothelial cells may exert on VSMC mechanical behavior was not specifically studied. It is known that this influence may be mostly related to changes in shear stress, which are directly sensed by these cells (37). VSMC behavior in vitro may not be completely extrapolated to their properties in vivo, but restricting culture passage and selecting a primary culture may have helped in preserving cell phenotype (10). Vessel intrinsic tone, which is regulated by adrenergic stimulus (46), may influence VSMC rigidity by modifying substrate stiffness (3). In our study, the influence of this factor on VSMC behavior was not directly evaluated. Finally, our choice in focusing on the media layer was an attempt to evaluate the environment surrounding terminally differentiated VSMCs, which might have a direct influence on their behavior, but it is known that adventitia may also contribute to vessel mechanics.

In conclusion, VSMCs are heterogeneous in terms of viscoelasticity and the amount of cytoskeletal proteins expressed along the arterial tree, their mechanical phenotype possibly being influenced by ECM characteristics (amount and composition) as well as being modulated by cyclic circumferential stress applied to vessel walls by blood flow.

ACKNOWLEDGMENTS

We thank Sônia Regina Yokomizo, Márcio José Chaves, and Ana Lúcia Garippo for the technical help.

GRANTS

This work was supported by Grant No. 2012/21103-0, São Paulo Research Foundation (FAPESP), and Fleury Group, São Paulo, Brazil.

DISCLOSURES

No conflicts of interest, financial or otherwise, are declared by the author(s).

AUTHOR CONTRIBUTIONS

Author contributions: C.L.D., J.E.K., A.M.A., and A.C.P. conception and design of research; C.L.D., G.V., I.S.W., L.C.G.C., R.D., J.M.d.M.-L.F., V.M.C., and K.H.M.C. performed experiments; C.L.D., G.V., E.H.Z., L.C.G.C., R.D., J.M.d.M.-L.F., V.M.C., K.H.M.C., A.M.A., and A.C.P. analyzed data; C.L.D., G.V., E.H.Z., L.C.G.C., R.D., J.M.d.M.-L.F., V.M.C., K.H.M.C., J.E.K., A.M.A., and A.C.P. interpreted results of experiments; C.L.D. and I.S.W. prepared figures; C.L.D. drafted manuscript; C.L.D., J.E.K., and A.C.P. edited and revised manuscript; E.H.Z., J.E.K., and A.C.P. approved final version of manuscript.

REFERENCES

1. **Berry CL, Greenwald SE, Rivett JF.** Static mechanical properties of the developing and mature rat aorta. *Cardiovasc Res* 9: 669–678, 1975.
2. **Bieler FH, Ott CE, Thompson MS, Seidel R, Ahrens S, Epari DR, Wilkening U, Schaser KD, Mundlos S, Duda GN.** Biaxial cell stimulation: A mechanical validation. *J Biomech* 42: 1692–1696, 2009.
3. **Brown XQ, Bartolak-Suki E, Williams C, Walker ML, Weaver VM, Wong JY.** Effect of substrate stiffness and PDGF on the behavior of vascular smooth muscle cells: implications for atherosclerosis. *J Cell Physiol* 225: 115–122, 2010.
4. **Bryant PW, Zheng Q, Pumiglia KM.** Focal adhesion kinase is a phospho-regulated repressor of Rac and proliferation in human endothelial cells. *Biol Open* 1: 723–730, 2012.
5. **Camargo M, Intasqui Lopes P, Del Giudice PT, Carvalho VM, Cardozo KH, Andreoni C, Fraietta R, Bertolla RP.** Unbiased label-free quantitative proteomic profiling and enriched proteomic pathways in

seminal plasma of adult men before and after varicocelectomy. *Hum Reprod* 28: 33–46, 2013.
6. **Campos LC, Miyakawa AA, Barauna VG, Cardoso L, Borin TF, Dallan LA, Krieger JE.** Induction of CRP3/MLP expression during vein arterialization is dependent on stretch rather than shear stress. *Cardiovasc Res* 83: 140–147, 2009.
7. **Chapman GB, Durante W, Hellums JD, Schafer AI.** Physiological cyclic stretch causes cell cycle arrest in cultured vascular smooth muscle cells. *Am J Physiol Heart Circ Physiol* 278: H748–H754, 2000.
8. **Chen C, Krishnan R, Zhou E, Ramachandran A, Tambe D, Rajendran K, Adam RM, Deng L, Fredberg JJ.** Fluidization and resolidification of the human bladder smooth muscle cell in response to transient stretch. *PLoS One* 5: e12035, 2010.
9. **Colo GP, Hernandez-Varas P, Lock J, Bartolome RA, Arellano-Sanchez N, Stromblad S, Teixido J.** Focal adhesion disassembly is regulated by a RIAM to MEK-1 pathway. *J Cell Sci* 125: 5338–5352, 2012.
10. **Dinardo CL, Venturini G, Omae SV, Zhou EH, da Motta-Leal-Filho JM, Dariolli R, Krieger JE, Alencar AM, Costa Pereira A.** Vascular smooth muscle cells exhibit a progressive loss of rigidity with serial culture passaging. *Biorheology* 49: 365–373, 2012.
11. **Doran AC, Meller N, McNamara CA.** Role of smooth muscle cells in the initiation and early progression of atherosclerosis. *Arterioscler Thromb Vasc Biol* 28: 812–819, 2008.
12. **Fabry B, Maksym GN, Shore SA, Moore PE, Panettieri RA, Butler JP, Fredberg JJ.** Selected contribution: time course and heterogeneity of contractile responses in cultured human airway smooth muscle cells. *J Appl Physiol* 91: 986–994, 2001.
13. **Gerrity RG, Cliff WJ.** The aortic tunica media of the developing rat. I. Quantitative stereologic and biochemical analysis. *Lab Invest* 32: 585–600, 1975.
14. **Halayko AJ, Solway J.** Molecular mechanisms of phenotypic plasticity in smooth muscle cells. *J Appl Physiol* 90: 358–368, 2001.
15. **Hao H, Ropraz P, Verin V, Camenzind E, Geinoz A, Pepper MS, Gabbiani G, Bochaton-Piallat ML.** Heterogeneity of smooth muscle cell populations cultured from pig coronary artery. *Arterioscler Thromb Vasc Biol* 22: 1093–1099, 2002.
16. **Harkness ML, Harkness RD, McDonald DA.** The collagen and elastin content of the arterial wall in the dog. *Proc R Soc Lond B Biol Sci* 146: 541–551, 1957.
17. **Holzapfel GA, Ogden RW.** Modelling the layer-specific three-dimensional residual stresses in arteries, with an application to the human aorta. *J R Soc Interface* 7: 787–799, 2010.
18. **Jackson CL, Schwartz SM.** Pharmacology of smooth muscle cell replication. *Hypertension* 20: 713–736, 1992.
19. **Jin L, Kern MJ, Otey CA, Wamhoff BR, Somlyo AV.** Angiotensin II, focal adhesion kinase, and PRX1 enhance smooth muscle expression of lipoma preferred partner and its newly identified binding partner palladin to promote cell migration. *Circ Res* 100: 817–825, 2007.
20. **Karnik SK, Brooke BS, Bayes-Genis A, Sorensen L, Wythe JD, Schwartz RS, Keating MT, Li DY.** A critical role for elastin signaling in vascular morphogenesis and disease. *Development* 130: 411–423, 2003.
21. **Katsumi A, Milanini J, Kiosses WB, del Pozo MA, Kaunas R, Chien S, Hahn KM, Schwartz MA.** Effects of cell tension on the small GTPase Rac. *J Cell Biol* 158: 153–164, 2002.
22. **Kawasaki T, Sasayama S, Yagi S, Asakawa T, Hirai T.** Non-invasive assessment of the age related changes in stiffness of major branches of the human arteries. *Cardiovasc Res* 21: 678–687, 1987.
23. **Kim S, Ip HS, Lu MM, Clendenin C, Parmacek MS.** A serum response factor-dependent transcriptional regulatory program identifies distinct smooth muscle cell sublineages. *Mol Cell Biol* 17: 2266–2278, 1997.
24. **Kochova P, Kuncova J, Sviglerova J, Cimrman R, Miklikova M, Liska V, Tonar Z.** The contribution of vascular smooth muscle, elastin and collagen on the passive mechanics of porcine carotid arteries. *Physiol Meas* 33: 1335–1351.
25. **Kuang SQ, Kwartler CS, Byanova KL, Pham J, Gong L, Prakash SK, Huang J, Kamm KE, Stull JT, Sweeney HL, Milewicz DM.** Rare, nonsynonymous variant in the smooth muscle-specific isoform of myosin heavy chain, MYH11, R247C, alters force generation in the aorta and phenotype of smooth muscle cells. *Circ Res* 110: 1411–1422.
26. **Lee RT, Yamamoto C, Feng Y, Potter-Perigo S, Briggs WH, Landschulz KT, Turi TG, Thompson JF, Libby P, Wight TN.** Mechanical strain induces specific changes in the synthesis and organization of proteoglycans by vascular smooth muscle cells. *J Biol Chem* 276: 13847–13851, 2001.
27. **Li W, Chen Q, Mills I, Sumpio BE.** Involvement of S6 kinase and p38 mitogen activated protein kinase pathways in strain-induced alignment and proliferation of bovine aortic smooth muscle cells. *J Cell Physiol* 195: 202–209, 2003.
28. **Lilly B, Olson EN, Beckerle MC.** Identification of a CArG box-dependent enhancer within the cysteine-rich protein 1 gene that directs expression in arterial but not venous or visceral smooth muscle cells. *Dev Biol* 240: 531–547, 2001.
29. **Lu X, Zhao JB, Wang GR, Gregersen H, Kassab GS.** Remodeling of the zero-stress state of femoral arteries in response to flow overload. *Am J Physiol Heart Circ Physiol* 280: H1547–H1559, 2001.
30. **Mijailovich SM, Kojic M, Zivkovic M, Fabry B, Fredberg JJ.** A finite element model of cell deformation during magnetic bead twisting. *J Appl Physiol* 93: 1429–1436, 2002.
31. **Park CY, Tambe D, Alencar AM, Trepat X, Zhou EH, Millet E, Butler JP, Fredberg JJ.** Mapping the cytoskeletal prestress. *Am J Physiol Cell Physiol* 298: C1245–C1252, 2010.
32. **Qiu H, Zhu Y, Sun Z, Trzeciakowski JP, Gansner M, Depre C, Resuello RR, Natividad FF, Hunter WC, Genin GM, Elson EL, Vatner DE, Meininger GA, Vatner SF.** Short communication: vascular smooth muscle cell stiffness as a mechanism for increased aortic stiffness with aging. *Circ Res* 107: 615–619, 2010.
33. **Reymond P, Bohraus Y, Perren F, Lazeyras F, Stergiopulos N.** Validation of a patient-specific one-dimensional model of the systemic arterial tree. *Am J Physiol Heart Circ Physiol* 301: H1173–H1182, 2011.
34. **Riveline D, Zamir E, Balaban NQ, Schwarz US, Ishizaki T, Narumiya S, Kam Z, Geiger B, Bershadsky AD.** Focal contacts as mechanosensors: externally applied local mechanical force induces growth of focal contacts by an mDia1-dependent and ROCK-independent mechanism. *J Cell Biol* 153: 1175–1186, 2001.
35. **Rosenquist TH, McCoy JR, Waldo KL, Kirby ML.** Origin and propagation of elastogenesis in the developing cardiovascular system. *Anat Rec* 221: 860–871, 1988.
36. **Saphirstein RJ, Gao YZ, Jensen MH, Gallant CM, Vetterkind S, Moore JR, Morgan KG.** The focal adhesion: a regulated component of aortic stiffness. *PLoS One* 8: e62461, 2013.
37. **Scott D, Tan Y, Shandas R, Stenmark KR, Tan W.** High pulsatility flow stimulates smooth muscle cell hypertrophy and contractile protein expression. *Am J Physiol Lung Cell Mol Physiol* 304: L70–L81, 2013.
38. **Thakar RG, Cheng Q, Patel S, Chu J, Nasir M, Liepmann D, Komvopoulos K, Li S.** Cell-shape regulation of smooth muscle cell proliferation. *Biophys J* 96: 3423–3432, 2009.
39. **Tojkander S, Gateva G, Lappalainen P.** Actin stress fibers–assembly, dynamics and biological roles. *J Cell Sci* 125: 1855–1864, 2012.
40. **Topouzis S, Majesky MW.** Smooth muscle lineage diversity in the chick embryo. Two types of aortic smooth muscle cell differ in growth and receptor-mediated transcriptional responses to transforming growth factor-beta. *Dev Biol* 178: 430–445, 1996.
41. **Trepat X, Deng L, An SS, Navajas D, Tschumperlin DJ, Gerthoffer WT, Butler JP, Fredberg JJ.** Universal physical responses to stretch in the living cell. *Nature* 447: 592–595, 2007.
42. **Wagenseil JE, Mecham RP.** Vascular extracellular matrix and arterial mechanics. *Physiol Rev* 89: 957–989, 2009.
43. **Watanabe I.** Fine structure of lamellated nerve endings in the gingiva of man and the Cebus apella monkey. *Okajimas Folia Anat Jpn* 59: 181–198, 1982.
44. **Wei S, Gao X, Du J, Su J, Xu Z.** Angiogenin enhances cell migration by regulating stress fiber assembly and focal adhesion dynamics. *PLoS One* 6: e28797, 2011.
45. **Yoshida T, Owens GK.** Molecular determinants of vascular smooth muscle cell diversity. *Circ Res* 96: 280–291, 2005.
46. **Zacharia J, Mauban JR, Raina H, Fisher SA, Wier WG.** High vascular tone of mouse femoral arteries in vivo is determined by sympathetic nerve activity via alpha1A- and alpha1D-adrenoceptor subtypes. *PLoS One* 8: e65969, 2013.
47. **Zhou EH, Krishnan R, Stamer WD, Perkumas KM, Rajendran K, Nabhan JF, Lu Q, Fredberg JJ, Johnson M.** Mechanical responsiveness of the endothelial cell of Schlemm's canal: scope, variability and its potential role in controlling aqueous humour outflow. *J R Soc Interface* 9: 1144–1155, 2012.